Incommensurate structures studied by a modified density-matrix renormalization-group method

A. Gendiar and A. Šurda
Institute of Physics, Slovak Academy of Sciences, Dúbravská cesta 9, SK-842 28 Bratislava, Slovak Republic
(Received 7 December 1999; revised manuscript received 8 February 2000)

A modified density-matrix renormalization-group (DMRG) method is introduced and applied to classical two-dimensional models: the anisotropic triangular nearest-neighbor Ising model and the anisotropic triangular next-nearest-neighbor Ising model. Phase diagrams of both models have complex structures and exhibit incommensurate phases. It was found that the incommensurate phase completely separates the disordered phase from one of the commensurate phases, i.e., the nonexistence of the Lifshitz point is conjectured in phase diagrams of both models with the DMRG method. It is shown that the DMRG method is also an effective-field approximation, but in spite of that it yields the correct value of the domain wall density critical exponent.

I. INTRODUCTION

In 1992 White[1] invented the density-matrix renormalization-group (DMRG) technique in real space which has been mostly used for diagonalization of one-dimensional (1D) quantum chain spin Hamiltonians. Three years later Nishino[2] applied this numerical technique to classical spin 2D models. The DMRG method is based on renormalization of the transfer matrix. It is a variational method that maximizes the partition function using a limited number of degrees of freedom and the variational state is written as a product of local matrices.[3]

A similar method (cluster transfer matrix method) for classical spin models was developed by one of us, where the variational state is written as a product of local functions.[4,5] In this paper we shall compare the results of both methods.

The DMRG technique proceeds in two steps. In the first one, the infinite system method (ISM) pushes both ends of the system from each other and enlarges the system by two sites at each iteration. In the second one, the finite system method (FSM), in which the system has fixed size, improves the values of calculated physical quantities by several left and right moves (sweeps) yielding very accurate results.[1]

DMRG has been used for many various quantum models. It provides results with remarkable accuracy for larger systems than it is possible to study using standard diagonalization methods. The 2D classical systems treated by the DMRG method exceeds the classical Monte Carlo approach in accuracy, speed, and size of the systems.[6] In spite of this, too few works have been still done for 2D classical spin models by the DMRG technique.[2,7,8] A further DMRG improvement of the classical systems is based on Baxter's corner transfer matrix,[9] the CTMRG,[10] and its generalization to any dimension.[11]

The aim of this paper is to investigate two classical models that exhibit incommensurate (IC) phases, namely, the anisotropic next-nearest-neighbor Ising (ANNNI) model[4] and the anisotropic triangular nearest-neighbor Ising (ATNNI) model.[12] The incommensurate phases were studied by many various theoretical approaches. The free fermion approximation revealed IC phase in 2D classical ANNNI model[13] (also[12] in the ATNNI model), 2D incommensurate crystals.[14] Incommensurate structures has been discussed in various topics: 2D C-IC phase transition,[15] 2D quantum ANNNI model,[16] ANNNI model in $d>2$ dimensions,[17] and by analyzing the 1D sine-Gordon model[18] where the authors found no Lifshitz point.

We develop a modified DMRG method which can be applied to more complicated systems, namely, to the ANNNI and ATNNI models. Both models are characterized by nonsymmetric transfer matrices. The way how to use the DMRG in that case is described in this paper. We show the modification of the DMRG for treating nonsymmetric transfer matrix in the ATNNI model, and discussed it in light of other approaches to the nonsymmetric transfer matrices or non-Hermitian quantum Hamiltonians.[19,20] In particular, the existence or nonexistence of the Lifshitz point in the ATNNI model will be studied and its phase diagrams will be constructed.

This paper is organized as follows. in Sec. II we compare two different applications of the DMRG technique. In Sec. III we describe the ATNNI and ANNNI models. Section IV contains the modified DMRG algorithm for the ATNNI model. In Sec. V we present our results and in Sec. VI the results will be summarized and discussed.

II. THE DMRG TECHNIQUE FOR 2D SPIN SYSTEMS

For special values of interaction constants both ATNNI and ANNNI models can be reduced to the Ising model. In this case we can compare our approximate DMRG calculations with the exact results for infinite 2D models.

Exact results can be relatively easily obtained for 1D models, e.g., strips of finite width. They provide a good opportunity for testing our methods, as well.

The DMRG technique as a numerical real-space method, is in fact always applied to finite systems. However, in dependence on the size of the system, it can yield approximate descriptions of 1D or 2D infinite systems.

In the case of relatively narrow strips the DMRG calculations are consistent with the exact calculations. They yield a zero-order parameter and reproduces well the largest and the second largest eigenvalues of the transfer matrix of the system. Comparison of the exact and approximate values for Ising and ATNNI models on a semi-infinite strip of width

TABLE I. Largest eigenvalues λ_1 and the second largest eigenvalues λ_2 of the transfer matrices calculated with the DMRG technique for the Ising model with periodic boundary conditions. The dimension of the transfer matrix N depends on the size of the block-spin variable (in Ref. 2). The last line of the table contains the eigenvalues of the transfer matrix obtained by the exact diagonalization method.

	Ising model with periodic boundary conditions			
	Ordered phase $T=2.1$		Disordered phase $T=2.4$	
N	λ_1	λ_2	λ_1	λ_2
400	$7.003\,316\,79\times10^6$	$6.918\,036\,4\times10^6$	$1.763\,794\,94\times10^6$	$1.547\,703\,4\times10^6$
1600	$7.039\,903\,43\times10^6$	$6.974\,229\,2\times10^6$	$1.767\,024\,61\times10^6$	$1.576\,984\,4\times10^6$
3600	$7.039\,918\,36\times10^6$	$6.974\,259\,5\times10^6$	$1.767\,043\,24\times10^6$	$1.577\,140\,6\times10^6$
6400	$7.040\,011\,44\times10^6$	$6.974\,313\,3\times10^6$	$1.767\,105\,92\times10^6$	$1.577\,173\,6\times10^6$
10 000	$7.040\,011\,46\times10^6$	$6.974\,313\,5\times10^6$	$1.767\,105\,93\times10^6$	$1.577\,174\,0\times10^6$
65 536	$7.040\,011\,65\times10^6$	$6.974\,314\,6\times10^6$	$1.767\,105\,98\times10^6$	$1.577\,179\,9\times10^6$

$L=16$ with periodic boundary conditions for various approximations are given in Tables I and II. We see that the first two eigenvalues of the superblock transfer matrices in the DMRG method are very close to the exact values despite small sizes of superblock matrices ($N\times N$) that are much less than the size of the exact T matrix (65536×65536) The calculations for the ATNNI model were performed at a moderate magnetic field $H=2$. At higher magnetic fields we frequently encountered problems with complex conjugated pairs of two largest transfer matrix eigenvalues in the DMRG calculations. Consequent symmetrizing of the density matrix (presented in Ref. 21) did not improve the calculations.

An 1D model at nonzero temperature does not display any phase transitions. Nevertheless, the value of the critical temperature for the corresponding 2D model can be found from finite-size scaling (FSS) considerations.[22] This approach represents the first of two methods we shall use for determination of the critical temperature. Its value for the Ising model, derived from comparing two rescaled semi-infinite strips of width $L=12$ and 14 with periodic boundary conditions, are the following.

(i) $T_c=2.269\,87$ from the exact eigenvalues of the transfer matrices of the size $N=4096$ and $N=16\,384$, (ii) $T_c=2.270\,08$ from the eigenvalues of the DMRG superblock transfer matrices of the size $N=1024$, comparing with the exact critical temperature of the 2D Ising model $T_c=2.269\,18\cdots$.[23]

The second method for determination of the critical temperature is provided by DMRG calculations on 2D systems, which is large in both directions. Here, below the critical temperature a spontaneous symmetry breaking occurs, i.e., the order parameter acquires nonzero values and tends to zero at the critical point. The DMRG method behaves in a mean-field-like manner. Now the critical temperature T_c can be determined directly and therefore no finite-size scaling is necessary. Its accuracy improves with the size of the superblock transfer matrix as follows: (i) $T_c=2.275$ for $N=1024$, (ii) $T_c=2.272$ for $N=3600$, (iii) $T_c=2.2692$ for $N=19\,600$.

For lower orders of approximation, the accuracy of the second method is worse than of the first one, but it converges faster to the exact value. For the ATNNI and ANNNI models in the phases with broken symmetry, the method explicitly gives the structure of a commensurate as well as an incommensurate phase. In contrast to the FSS method, it is also applicable for the high magnetic field region in the ATNNI model and we were able to investigate nearly the whole phase diagram of the model.

III. ATNNI AND ANNNI MODELS

A. The ATNNI model

We consider the two-dimensional classical Ising model with antiferromagnetic interactions between nearest neighbors on a triangular lattice (the ATNNI model). Its Hamiltonian is as follows:

TABLE II. The two largest eigenvalues λ_1 and λ_2 of the transfer matrix for the ATNNI model calculated by the DMRG technique for periodic boundary conditions. Data obtained by the exact diagonalization method are shown in the last line.

	ATNNI model with periodic boundary conditions			
	Commensurate phase $T=0.9,\ H=2.0$		Disordered phase $T=1.2,\ H=2.0$	
N	λ_1	λ_2	λ_1	λ_2
400	3.8724×10^{12}	2.4898×10^{11}	5.8940×10^9	1.0267×10^9
1600	4.0818×10^{12}	3.7378×10^{12}	6.9274×10^9	4.5860×10^9
3600	4.0503×10^{12}	3.7013×10^{12}	6.9235×10^9	4.5697×10^9
6400	4.0560×10^{12}	3.7033×10^{12}	6.9330×10^9	4.5120×10^9
10 000	4.0556×10^{12}	3.6996×10^{12}	6.9328×10^9	4.4892×10^9
65 536	4.0530×10^{12}	3.6884×10^{12}	6.9312×10^9	4.4368×10^9

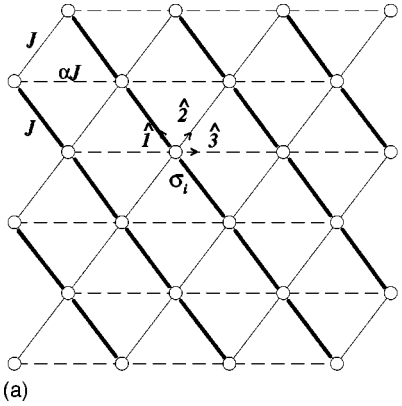

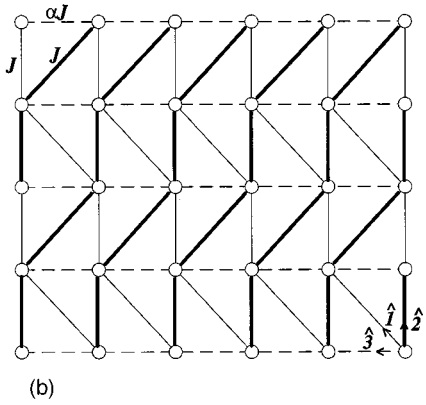

FIG. 1. (a) Triangular lattice of the ATNNI model. The incommensurate structure appears along the direction $\hat{3}$ (dashed lines). (b) For more convenient calculation the triangular lattice was transformed to a rectangular one. The transfer matrices are located between neighboring horizontal lines. Now directions $\hat{1}$ and $\hat{2}$ correspond to each other in both (a) and (b).

$$\mathcal{H}=\sum_i J\left(\sum_{\hat{\delta}=\hat{1},\hat{2}} \sigma_i\sigma_{i+\hat{\delta}}+\alpha\sigma_i\sigma_{i+\hat{3}}\right)-H\sum_i \sigma_i \qquad (1)$$

with $J>0$, $0<\alpha<1$, and the directions $\hat{1}$, $\hat{2}$, $\hat{3}$ where $\sigma_i=\pm 1$, as depicted in Fig. 1(a).

The partition function $\mathcal{Z}=\Sigma_{\{\sigma\}}e^{-\beta\mathcal{H}}$, where $\beta=(k_BT)^{-1}$, can be written as a product of two types of Boltzmann weights. Each Boltzmann weight $W_B(\sigma_1\sigma_2|\sigma_1'\sigma_2')$ is composed of four spins which interact among themselves as seen in Fig. 2.

The model is exactly solvable for the external magnetic field $H=0$. At nonzero temperature [$T_c\approx 1.55$ for $\alpha=0.4$ (Ref. 12)], it exhibits the second order phase transition. Throughout this paper all numerical calculations are performed at the fixed $\alpha=0.4$, $J=1$ and the dimensionless temperature T/J and dimensionless ratio H/T are used in order to compare our results with those obtained in (Ref. 12).

The numerical calculations are based on a diagonalization of two transfer matrices (in the next section, we will offer a more detailed description of their construction). For this purpose we used the rectangular lattice depicted Fig. 1(b) which is related to the initial triangular lattice of the ATNNI model as seen in Fig. 1(a). We identify direction $\hat{3}$ with the interaction αJ (Fig. 1). In this direction, the incommensurate modulation should appear. We will use the row-to-row transfer matrices.[12]

B. The ANNNI model

The ANNNI model is defined on the 2D triangular lattice with the nearest-neighbor ferromagnetic interactions $J_1<0$ for all three directions and a next-nearest-neighbor antiferromagnetic interaction $J_2>0$ in one of three directions only. (See Fig. 3). Its Hamiltonian can be written as

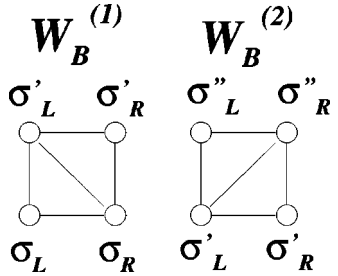

FIG. 2. Two kinds of Boltzmann weights differing from each other by orientation of diagonal interactions.

$$\mathcal{H}=\sum_i\left(\sum_{\hat{\delta}=\hat{1},\hat{2},\hat{3}} J_1\sigma_i\sigma_{i+\hat{\delta}}+J_2\sigma_i\sigma_{i+\hat{4}}\right). \qquad (2)$$

The ANNNI model is usually defined on the square lattice where the next-nearest-neighbor interactions are, in fact, equal to zero and the third-nearest-neighbor ones are nonzero and antiferromagnetic. Thus, the ANNNI model on the triangular lattice is the genuine anisotropic next-nearest-neighbor interaction model with nonzero next-nearest-neighbor interactions and vanishing third-nearest-neighbor ones. A frustration of the ANNNI model appears due to the competing interactions. The ANNNI model was mostly studied on the square lattice[24] but it shown in Ref. 4 that the properties of the ANNNI model on the triangular lattices remain essentially unchanged. A Boltzmann weight is composed of six spins $W_B(\sigma_1\sigma_2\sigma_3|\sigma_1'\sigma_2'\sigma_3')$ or graphically in Fig. 4.

The phase diagram of the ANNNI model (will be discussed in Sec. V) consists of four regions: a ferromagnetic phase with nonzero total magnetization, a commensurate phase $\langle 2\rangle$ with periodically alternating spin signs ($\cdots++--+--\cdots$), a paramagnetic phase, and an incommensurate phase located between the commensurate and paramagnetic phases.

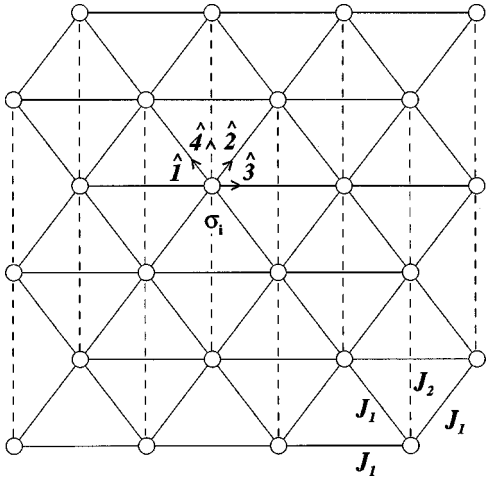

FIG. 3. The 2D ANNNI model on the triangular lattice. Directions $\hat{1}$, $\hat{2}$, and $\hat{3}$ characterize the ferromagnetic interaction J_1. The next-nearest-neighbor antiferromagnetic interaction J_2 (dashed line) acts in the direction $\hat{4}$ in which the incommensurate phase appears.

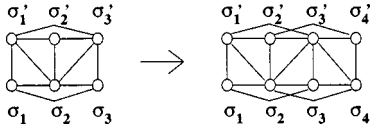

FIG. 4. The six-spin Boltzmann weights of the ANNNI model differing from each other by orientation of the diagonal interactions. In the DMRG calculation the Boltzmann weight defined on the eight-spin cluster was used. It is composed of two overlapping six-spin Boltzmann weights.

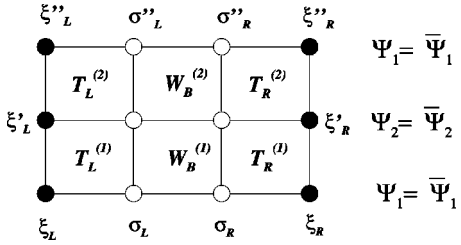

FIG. 5. Ψ_1, $\bar{\Psi}_1$ are the right and left eigenvectors that correspond to the largest eigenvalue of the superblock transfer matrices ${}^iT^{(1)}={}^iT_L^{(1)}{}^iW_B^{(1)}{}^iT_R^{(1)}$, and ${}^iT^{(2)}={}^iT_L^{(2)}{}^iW_B^{(2)}{}^iT_R^{(2)}$, respectively. Vectors Ψ_2 and $\bar{\Psi}_2$ are used for the calculation of the density matrix in each DMRG iteration.

IV. MODIFICATION OF THE DMRG ALGORITHM

The DMRG algorithm for quantum models introduced by White[1] was modified and applied for 2D classical lattice models by Nishino.[2] Since the ATNNI and ANNNI models on the triangular lattice lead to nonsymmetric transfer matrices and incommensurate phases, Nishino's approach has to be modified further. We shall pursue the second approach discussed in Sec. II—the DMRG method applied to very wide strips where the spontaneous symmetry breaking occurs.

The DMRG method replaces the exact row-to-row transfer matrix of a strip, which is a product of plaquette Boltzmann weights, by a set of much smaller superblock transfer matrices for every plaquette. The superblock transfer matrix consists of the Boltzmann weight ${}^iW_B$ of the plaquette i multiplied by left and right transfer matrices (blocks) ${}^iT_L$, ${}^iT_R$ which replace all the remaining plaquette Boltzmann weights of the exact transfer matrix to the left and right from the plaquette. The left and right transfer matrices are indexed by left and right spins $\sigma_{L,R}=\pm 1$ of the plaquette, respectively, and by block-spin variables $\xi=1,\ldots,m$. The number of spin components m determines the order of the approximation. For a modulated phase, ${}^iT_L$ and ${}^iT_R$ differ for each plaquette. In the FSM, they are calculated self-consistently from the transfer matrices corresponding to the neighboring plaquettes. The left block ${}^{i+1}T_L$ is obtained from ${}^iT_L^iW_B$ after a reduction of its matrix size to the original value in a proper way. The right block ${}^{i-1}T_R$ is similarly calculated from ${}^iW_B^iT_R$. A calculation of the left and right transfer matrices is performed iteratively in the course of a number of sweeps across the strip.

The reduction of the size of the transfer matrices is based on density matrices that are constructed from the left and right [or in Figs. 1(b) and 5 rather upper and lower] eigenvectors of the superblock matrix.[1] The procedure described above for homogeneous phases and symmetric transfer matrices is thoroughly explained in Ref. 2. For the ATNNI and ANNNI models the method should be slightly modified because the transfer matrices are not symmetric and the structure is modulated in both directions, in one of them, incommensurately. It is convenient to choose the strip perpendicularly to the direction of the incommensurate modulation with commensurate structure along the strip, i.e., the strip is orientated in the vertical direction of the lattice shown in Fig. 1(b). It is seen that there are two different row-to-row nonsymmetric transfer matrices in the strip. One transfer matrix is constructed from the Boltzmann weight $W_B^{(1)}$ and the other one from the $W_B^{(2)}$ [Figs. 1(b) and 5].

The number of superblock transfer matrices should be equal to 2 (at least), since there are the two different Boltzmann weights in the model. For the DMRG with spontaneous symmetry breaking and spatially modulated structures, they may be different for each plaquette of the lattice. The density matrices can be constructed either from the eigenvectors of the superblock transfer matrices or from functions obtained by an iterative procedure $\Psi_j=\Pi_{k=1}^{j}T^{(k)}\Psi_{\text{init}}$ starting from Ψ_{init} given by suitable boundary conditions. For a homogeneous structure and large j the function Ψ_j is identical to the eigenvector of the superblock T.

All the commensurate structures have the period 2 for the ATNNI model in the direction of the strip. Therefore, we use two superblock transfer matrices $T^{(1)}=T_L^{(1)}W_B^{(1)}T_R^{(1)}$ and $T^{(2)}=T_L^{(2)}W_B^{(2)}T_R^{(2)}$ shown in Fig. 5. They are dependent on the position of the plaquette in the horizontal direction (perpendicular to the strip). Similarly, as a result of the iteration procedure we obtain two different functions Ψ_j for j large enough. Let us denote the Ψ_1 as an eigenvector of the matrix $T^{(2)}T^{(1)}$ for j even and the Ψ_2 as another eigenvector of the matrix product $T^{(1)}T^{(2)}$ for j odd. These both combined matrices are already symmetric and their right and left eigenvectors, Ψ and $\bar{\Psi}$, respectively, are identical.

Writing down the spin variables explicitly, the right eigenvectors are given by the equation

$$\sum_{\xi_L\sigma_L\sigma_R\xi_R} T(\xi_L''\sigma_L''\sigma_R''\xi_R''|\xi_L\sigma_L\sigma_R\xi_R)\Psi_1(\xi_L\sigma_L\sigma_R\xi_R) = \lambda\Psi_1(\xi_L''\sigma_L''\sigma_R''\xi_R''), \tag{3}$$

where

$$T(\xi_L''\sigma_L''\sigma_R''\xi_R''|\xi_L\sigma_L\sigma_R\xi_R) = \sum_{\xi_L'\sigma_L'\sigma_R'\xi_R'} T^{(2)}(\xi_L''\sigma_L''\sigma_R''\xi_R''|\xi_L'\sigma_L'\sigma_R'\xi_R') \times T^{(1)}(\xi_L'\sigma_L'\sigma_R'\xi_R'|\xi_L\sigma_L\sigma_R\xi_R). \tag{4}$$

The eigenvectors at the odd rows Ψ_2 follow directly from Ψ_1

$$\Psi_2 = T^{(1)}\Psi_1. \tag{5}$$

The optimum size reduction of the matrix ${}^{i}T_L\,{}^{i}W_B$ is performed by multiplying both sides by rectangular matrices consisting of several eigenvectors of a density matrix that corresponds to its largest eigenvalues.[1,2] The density matrix at a row j is constructed from the left and right eigenvectors $\Psi_j, \overline{\Psi}_j$ (Ref. 5) of transfer matrices with their left and right spins, respectively, lying on the row. For modulated commensurate structures of a period p, the successive functions Ψ_j are not the eigenvectors of one transfer matrix but of a product of p transfer matrices. As for the ATNNI model we have two different kinds of rows and different left and right transfer matrices in superblocks, we need four different density matrices. The left density matrices have the following forms:

$$\rho_L^{(1)}(\xi_L^a\sigma_L^a|\xi_L^b\sigma_L^b) = \sum_{\sigma_R^c\xi_R^c} \Psi_1(\xi_L^a\sigma_L^a\sigma_R^c\xi_R^c)\overline{\Psi}_1(\xi_L^b\sigma_L^b\sigma_R^c\xi_R^c), \tag{6}$$

$$\rho_L^{(2)}({\xi'}_L^a{\sigma'}_L^a|{\xi'}_L^b{\sigma'}_L^b) = \sum_{{\sigma'}_R^c{\xi'}_R^c} \Psi_2({\xi'}_L^a{\sigma'}_L^a{\sigma'}_R^c{\xi'}_R^c)\overline{\Psi}_2({\xi'}_L^b{\sigma'}_L^b{\sigma'}_R^c{\xi'}_R^c). \tag{7}$$

In the expressions for the right ones, the summation is performed over the left spins. The functions Ψ_j and $\overline{\Psi}_j$ are identical that is why the density matrices in Eqs. (6) and (7) are symmetric. Here we should emphasize that the right blocks T_R are not mirror reflections of the left blocks T_L as they were in the standard approach.[1]

The choice of the density matrices according to Eqs. (6) and (7) corresponds to the requirement of the best approximation of density matrices at each row in further calculations. In this case the density matrices might be generally nonsymmetric. In 1D calculations with nonsymmetric Hamiltonians[19,20] the density matrices were also chosen as symmetric but different for each side of the Hamiltonian or the same, but taken as an average of the left and right ones. This choice is closer to the original White's approach where the goal is to find the best possible approximation for the left and right eigenvectors of the Hamiltonian (transfer matrix). For two-dimensional models with nonzero temperature the calculation is aimed at thermal averages of physical quantities, for which good values of density matrix are decisive. Thus, our approach with potentially nonsymmetric transfer matrices we reckon as the best one.

By diagonalization of the left symmetric density matrix one obtains a matrix of orthonormal eigenvectors O_L:

$$Q_L(k|\xi\sigma)\rho_L^{(1)}(\xi\sigma|\xi'\sigma')O_L(\xi'\sigma'|l) = \omega_k\delta_{kl}, \tag{8}$$

where Q_L is transposed O_L and the eigenvalues ω_k satisfies the relation

$$\sum_k \omega_k = 1. \tag{9}$$

Analogously, we repeat this procedure for the density matrices $\rho_L^{(2)}$ and $\rho_R^{(2)}$ in order to obtain matrices Q_L', O_L', Q_R', and O_R'. Discarding half eigenvectors in the matrices Q and O that correspond to the smallest eigenvalues ω_k, the matrices O and Q can be used as the reduction matrices in the calculation of ${}^{i+1}T_L^{(1)\mathrm{new}}$ via

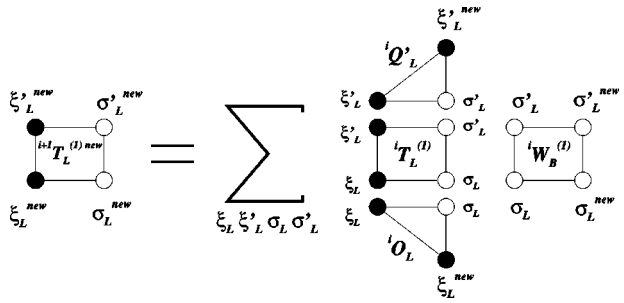

FIG. 6. Schematically written Eq. (10) which is used for computing the new left renormalized transfer matrix $T_L^{(1)\mathrm{new}}$ from the old one $T_L^{(1)}$.

$$\begin{aligned} {}^{i+1}T_L^{(1)\mathrm{new}}({\xi'}_L^{\mathrm{new}}{\sigma'}_L^{\mathrm{new}}|\xi_L^{\mathrm{new}}\sigma_L^{\mathrm{new}}) \\ = \sum_{\xi_L\xi_L'\sigma_L\sigma_L'} {}^{i}Q_L'({\xi'}_L^{\mathrm{new}}|\xi_L'\sigma_L')\,{}^{i}T_L^{(1)}(\xi_L'\sigma_L'|\xi_L\sigma_L) \\ \times {}^{i}W_B^{(1)}(\sigma_L'{\sigma'}_L^{\mathrm{new}}|\sigma_L\sigma_L^{\mathrm{new}})\,{}^{i}O_L(\xi_L\sigma_L|\xi_L^{\mathrm{new}}). \end{aligned} \tag{10}$$

Generalization for the right block is straightforward. The graphical representation of Eq. (10) is in Fig. 6. Notice that at this step (Fig. 6) the reduction matrix O_L is obtained by diagonalization of the density matrix $\rho_L^{(1)}$ whereas the matrix Q_L' yields from the diagonalization of the density matrix $\rho_L^{(2)}$. Knowing the functions Ψ_1, Ψ_2, $\overline{\Psi}_1$, and $\overline{\Psi}_2$ various physical quantities can be found, e.g., site magnetization used in further calculations

$$\langle\sigma_L\rangle = \sum_{\xi_L\sigma_L\sigma_R\xi_R} \Psi_1(\xi_L\sigma_L\sigma_R\xi_R)\sigma_L\overline{\Psi}_1(\xi_L\sigma_L\sigma_R\xi_R). \tag{11}$$

The superblock transfer matrix needs to be slightly changed for the ANNNI model. The left and right block transfer matrices have two spins more. The Boltzmann weight is defined on a plaquette of six spins. We have constructed the superblock transfer matrix T from the two block transfer matrices and the two overlapped Boltzmann weight (Fig. 4) as follows:

$$\begin{aligned} T(\xi_L\sigma_1\sigma_2\sigma_3\sigma_4\xi_R|\xi_L'\sigma_1'\sigma_2'\sigma_3'\sigma_4'\xi_R') \\ = T_L(\xi_L\sigma_1\sigma_2|\xi_L'\sigma_1'\sigma_2')W_B^{(1)}(\sigma_1\sigma_2\sigma_3|\sigma_1'\sigma_2'\sigma_3') \\ \times W_B^{(2)}(\sigma_2\sigma_3\sigma_4|\sigma_2'\sigma_3'\sigma_4')T_R(\sigma_3\sigma_4\xi_R|\sigma_3'\sigma_4'\xi_R'). \end{aligned} \tag{12}$$

V. RESULTS

Properties of the ANNNI model on the triangular lattice were calculated recently[4] by the cluster transfer matrix method.[27] The results were consistent with numerous calcu-

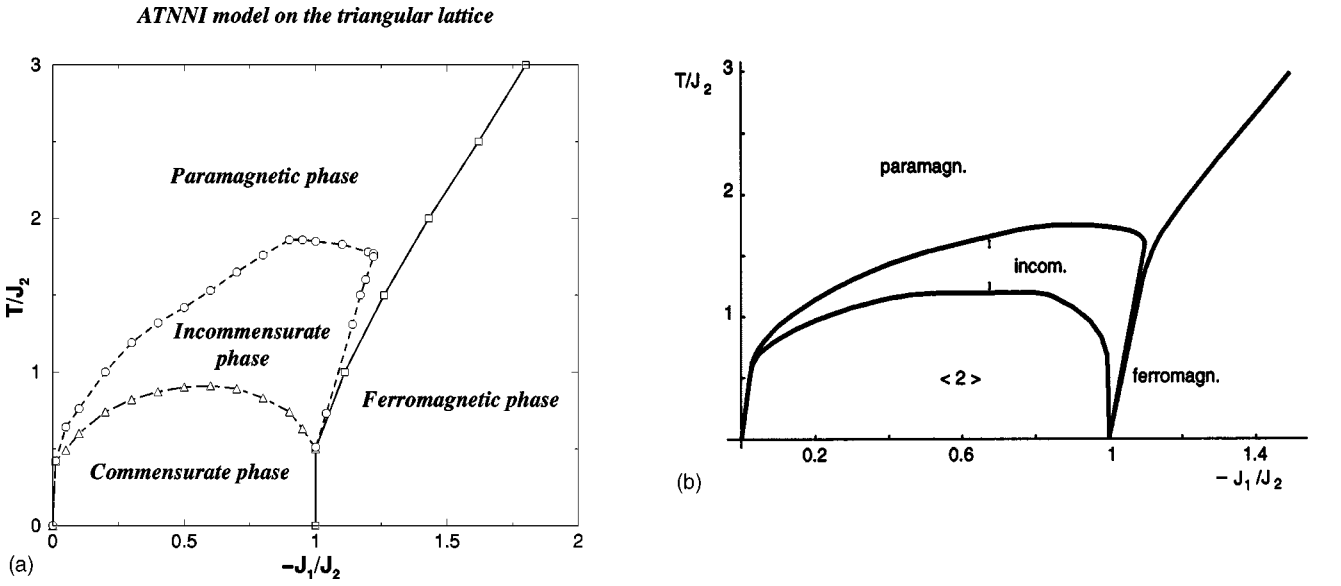

FIG. 7. (a) The phase diagram of the ANNNI model obtained by the DMRG method for relatively small superblock transfer-matrix size ($N=400$). After the superblock transfer-matrix size is increased, the IC region becomes narrower and the para-IC phase transition line is shifted to lower temperatures; (b) phase diagram from the cluster transfer matrix method in Ref. 4.

lations of the ANNNI model on the square lattice. To compare performance of the DMRG method for incommensurate (IC) structures with other methods we calculated the phase diagram of the ANNNI model shown in Fig. 7(a). The resulting diagram is in accordance with previous calculations[4] [Fig. 7(b)]. We have confirmed general opinion that there is no Lifshitz point on the ferromagnetic and paramagnetic phase transition line.

The region of the IC structure comes out from the DMRG rather wide, however, we have used a low-order approximation ($N=400$). For higher-order approximations the IC-phase region becomes narrower.

In addition to the critical temperature and the free energy also the critical exponents of Ising and ANNNI model were calculated. As expected, DMRG, as an effective-field approximation, yields classical values for all the critical exponents of the Ising model. Nevertheless, the critical exponent of the domain wall density at C-IC phase transition obtained from our DMRG approach has a nonclassical value 0.502 ± 0.003 close to the Pokrovsky-Talapov value 1/2,[25] which is assumed to be exact. Standard mean-field approximations give a logarithmic singularity at the critical line.[26] We explain this by a correct treatment of narrow-domain-wall meandering near the phase transition line by our large clusters. The resulting mean domain walls are straight, but, due to the summation over all spin values of the clusters, the wall meandering is involved in the calculation. The DMRG method reproduces the results of the domain wall theory well though no domain walls are explicitly introduced in it.

The phase diagram of the ATNNI model (in Fig. 8) consists of four regions (two different commensurate phases, incommensurate and disordered phase). Characteristic spin structures of both commensurate $\langle I \rangle$ and $\langle \mathrm{II} \rangle$ phases of the triangular lattice [Fig. 1(a)] are shown in the insets of the same phase diagram.

The phases $\langle I \rangle$ and $\langle \mathrm{II} \rangle$ consists of two and three different sublattices with a constant magnetization, respectively. In the IC phase, the magnetization of each sublattice is periodically modulated and the sublattices become equivalent to each other. That is why we only plot the magnetization of one of the sublattices in some of the following Figs. 9 and 10).

The phase diagram was derived from calculation of magnetization. The DMRG method with spontaneous symmetry breaking yields directly the space modulation of the magnetization which enables us to identify the phase unambiguously. In practical calculations, it is enough to observe the behavior of the largest eigenvalues of the superblock matrix. The period of their spatial modulation is the same as the period of the structure.

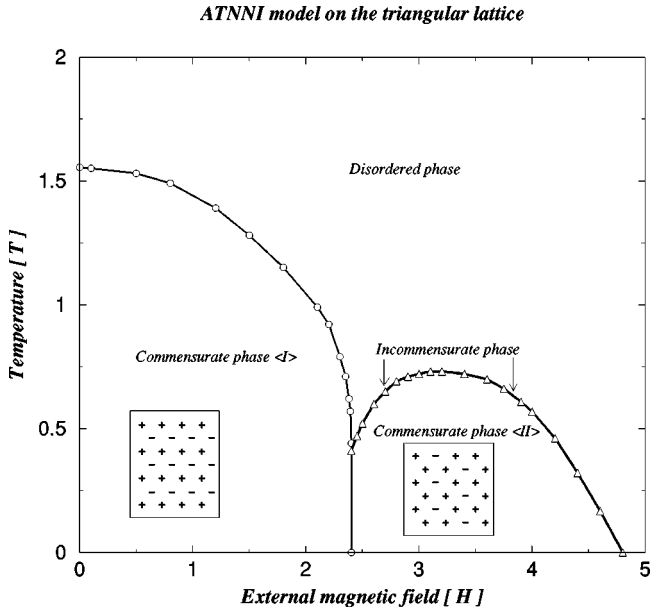

FIG. 8. The entire phase diagram of the ATNNI model is constructed by the DMRG technique. The incommensurate phase appears in narrow region located between the disordered phase and the commensurate phase $\langle \mathrm{II} \rangle$ for $2.4<H<4.8$. The ATNNI model is highly degenerated for $H=2.4$. The ATNNI model is highly degenerated for $H=2.4$.

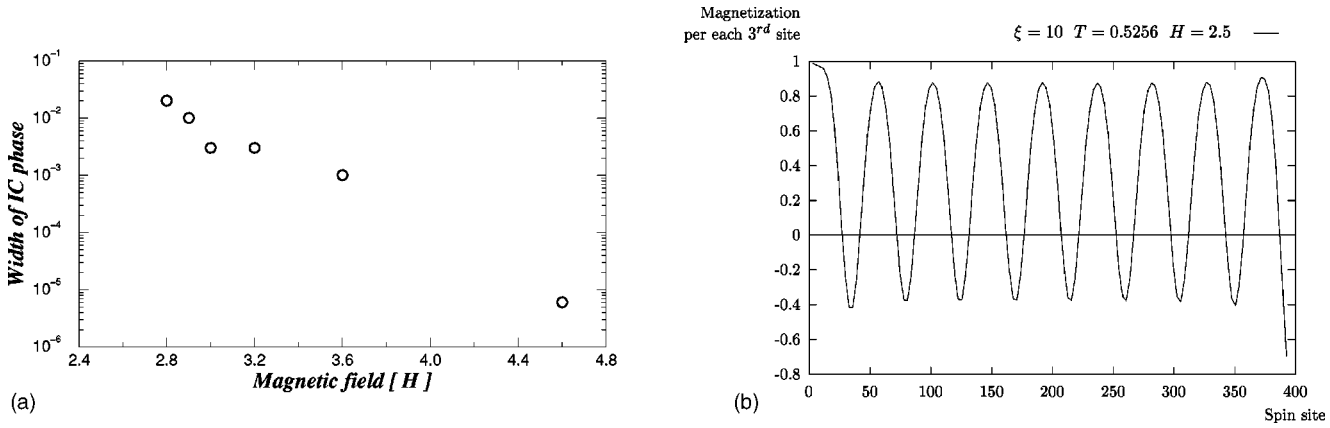

FIG. 9. (a) The width of the incommensurate phase measured in units of temperature vs external magnetic field H. With increasing field H the distance between the disordered and commensurate phases $\langle \mathrm{II} \rangle$ becomes shorter. (b) Measured magnetization per each third spin site using Eq. (11) inside the incommensurate phase as a function of the spin position on the lattice for $H=2.5$ and $T=0.5256$.

The incommensurate structure is floating, i.e., it is not fixed to the underlying lattice. In our calculation with spontaneous symmetry breaking, one of the infinitely many positions of the incommensurate wave is chosen at the beginning of the calculation and it remains fixed during the whole further calculation.

We have found the incommensurate structure practically along the whole border between the commensurate $\langle \mathrm{II} \rangle$ phase and the disordered phase. However, in two regions the calculations were inconclusive.

(i) The high degeneracy of the ground state at $H=2.4$ and $T<0.4$ (Ref. 12) has also caused highly degenerate largest eigenvalues of the superblock transfer matrix, and our method did not converge to any periodic structure for magnetic fields between 2.40 and 2.41 at low temperatures.

(ii) The other region is located at the high-magnetic-field end $H\approx 4.8$ and $T<0.1$ of the phase diagram. Here, the incommensurate phase is extremely narrow [Fig. 9(a)] and it has a very large period [Fig. 10(b)]. Moreover, due to the proximity of the second-order phase transition line, the convergence is very slow.

We have started the calculations with the ISM where the superblock transfer matrix is constructed from left and right transfer matrices of the *previous iteration step*. After a large number of iterations were performed, we obtained a final result for commensurate structures including the disordered phase. For the incommensurate structure it is necessary to perform afterwards some sweeps of the FSM in order to improve results that smooth the magnetization profile of the spin wave. The IC structure appears already after the application of the ISM but the correct shape of the magnetization is acquired after the FSM, only.

The shape of period of the IC structure changes with magnetic field H and temperature T. The period of the IC structure increases with the increasing magnetic field and decreasing temperature. At low temperatures (close to the $\langle \mathrm{II} \rangle$-IC phase transition line) the structure consists of wide domains of the phase $\langle \mathrm{II} \rangle$ separated by narrow domain walls. At higher temperatures near to disorder-IC transition, the domain walls become wider, the period shorter and the structure acquires a sinusoidal-like shape.

Both phase transitions are continuous. Inverse period of

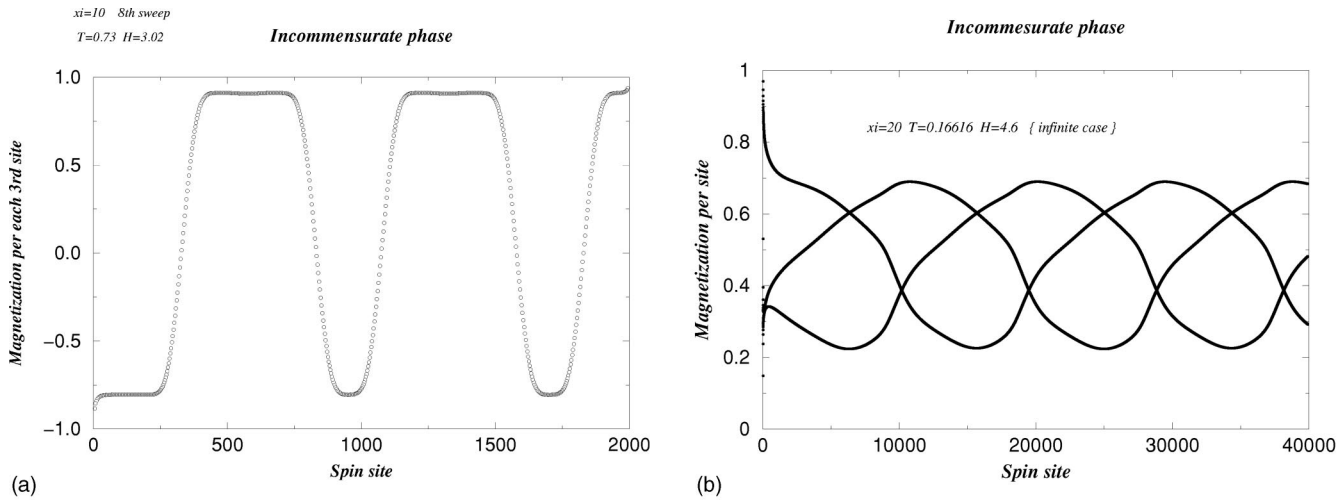

FIG. 10. (a) Magnetization vs position measured on the lattice inside the IC phase on each third site for $H=3.02$ and $T=0.73$. (b) IC phase obtained for the large magnetic field $H=4.6$ was found for temperatures $0.166\,158<T<0.166\,162$. The magnetization is measured on each site. All three spin waves are plotted.

the structure and wave amplitude tend to zero at the ⟨II⟩-IC and disorder-IC phase transition lines, respectively. It should be noted that the notions of low and high temperatures must be understood within an extremely narrow temperature interval where the IC phase exists.

The effect of magnetic field on the IC phase is similar (but inverse) to the temperature effects. Low magnetic field (near 2.4) enhances the high temperature effects, while the high magnetic field (near 4.8) the low temperature ones.

For the magnetic field H close to the value of 4.8, the period is very long, that is why we were able to perform the ISM only with an incorrect magnetization shape which would need a further improvement with the FSM [Fig. 10(b)].

Our calculations converged to the stable periodic solution at the most part of the commensurate ⟨II⟩-disordered phase borders. Here the IC phase has been found everywhere. This fact leads us to a conjecture (contrary to Ref. 12) that the Lifshitz point does not exists in the ATNNI model.

VI. SUMMARY

The DMRG method has been used to investigate incommensurate structures in the 2D classical model. We found that it reproduces the previous results for the ANNNI model well. In the case of the ATNNI model it has shown much better performance in regions where the previous approaches (the cluster transfer matrix method[27,28] near $H=2.4$ and the free-fermion approximation[12] for $H>3$) have failed. On the basis of scaling properties of Monte Carlo calculations and the exact diagonalization of finite strips, the authors of Ref. 12 concluded that at $H\cong 3$ the IC structure disappears and at higher fields H the direct phase transition between commensurate ⟨II⟩ and disordered phases is continuous.

We have observed the IC phase everywhere between the disordered and commensurate ⟨II⟩ phases, i.e., we have found no Lifshitz point where the three phases meet: commensurate, incommensurate, and disordered. Nevertheless, measured widths of the IC phase are extremely small at large H and exponentially tend to zero at $H=4.8$. As the width of the IC phase gets narrower for the high-order approximations we cannot completely exclude the scenario of Domany and Schaub.[12] Our belief in correct description of incommensurate phases by the DMRG technique is supported by the reproduction of the ANNNI phase diagram with generally expected features.

ACKNOWLEDGMENTS

This work has been supported by Slovak Grant Agency, Grant No. 2/4109/98. We would like to thank the organizers of the DMRG Seminar and Workshop in Dresden for the opportunity to participate in the meetings, especially for the useful discussion with T. Nishino and I. Peschel. A. G. also thanks P. Markoš for useful discussions and comments.

[1] S. R. White, Phys. Rev. Lett. **69**, 2863 (1992); Phys. Rev. B **48**, 10 345 (1993).
[2] T. Nishino, J. Phys. Soc. Jpn. **64**, 3598 (1995); T. Nishino, T. Hikihara, K. Okunishi, and Y. Hieida, Int. J. Mod. Phys. B **13**, 1 (1999).
[3] S. Östlund and S. Rommer, Phys. Rev. Lett. **75**, 3537 (1995); Phys. Rev. B **55**, 2164 (1997); K. Okunishi, Y. Hieida, and Y. Akutsu, cond-mat/9810239 (unpublished).
[4] P. Pajerský and A. Šurda, J. Phys. A **30**, 4187 (1997).
[5] A. Šurda, Acta Phys. Slov. **49**, 325 (1999).
[6] K. Hallberg, cond-mat/9910082 (unpublished).
[7] E. Carlon and A. Drzewiński, Phys. Rev. Lett. **79**, 1591 (1997).
[8] T. Nishino and K. Okunishi, J. Phys. Soc. Jpn. **64**, 4084 (1995).
[9] R. Baxter, J. Math. Phys. **9**, 650 (1968); J. Stat. Phys. **19**, 461 (1978).
[10] T. Nishino and K. Okunishi, J. Phys. Soc. Jpn. **65**, 891 (1996); **66**, 3040 (1997); T. Nishino, K. Okunishi, and M. Kikuchi, Phys. Lett. A **213**, 69 (1996).
[11] T. Nishino and K. Okunishi, J. Phys. Soc. Jpn. **67**, 3066 (1998).
[12] E. Domany and B. Schaub, Phys. Rev. B **29**, 4095 (1983).
[13] J. Villain and P. Bak, J. Phys. (France) **42**, 657 (1981).
[14] V. L. Pokrovsky and A. L. Talapov, Phys. Rev. Lett. **42**, 65 (1979).
[15] H. J. Schultz, Phys. Rev. B **22**, 5274 (1980).
[16] M. N. Barber and P. M. Duxbury, J. Phys. A **14**, L251 (1981).
[17] M. E. Fischer and W. Selke, Phys. Rev. Lett. **44**, 1502 (1980).
[18] F. D. M. Haldane, P. Bak, and T. Bohr, Phys. Rev. B **28**, 2743 (1983).
[19] Y. Hieida, J. Phys. Soc. Jpn. **67**, 369 (1998); Y. Hieida, K. Okunishi, and Y. Akutsu, New J. Phys. **1**, 7.1 (1999).
[20] T. Nishino and N. Shibata, J. Phys. Soc. Jpn. **68**, 3501 (1999); N. Shibata, *ibid.* **66**, 2221 (1997); X. Wang and T. Xiang, Phys. Rev. B **56**, 5061 (1997); R. J. Burssil, T. Xiang, and G. A. Gehring, J. Phys.: Condens. Matter **8**, L583 (1996); K. Maisinger and U. Schollwöck, Phys. Rev. Lett. **81**, 445 (1998).
[21] E. Carlon, M. Henkel, and U. Schollwöck, Eur. Phys. J. B **12**, 99 (1999).
[22] P. Nightingale, J. Appl. Phys. **53**, 7927 (1982).
[23] R. J. Baxter, *Exactly Solved Models in Statistical Physics* (Academic Press, London, 1982).
[24] W. Selke, Phys. Rep. **170**, 213 (1988); W. Selke, *Phase Transition and Critical Phenomena* (Academic, New York, 1992), Vol. 15.
[25] M. den Nijs, in *Phase Transition and Critical Phenomena*, edited by C. Domb and J. L. Lebowitz (Academic, London, 1988), Vol. 12, pp. 220–333.
[26] P. Bak, Rep. Prog. Phys. **45**, 587 (1982).
[27] I. Karasová and A. Šurda, J. Stat. Phys. **70**, 675 (1993).
[28] L. Tóth and A. Šurda (unpublished).